

The Volcanic Signal in Surface Temperature Observations

ALAN ROBOCK AND JIANPING MAO

Department of Meteorology, University of Maryland, College Park, Maryland

(Manuscript received 2 July 1993, in final form 27 September 1994)

ABSTRACT

Climate records of the past 140 years are examined for the impact of major volcanic eruptions on surface temperature. After the low-frequency variations and El Niño/Southern Oscillation signal are removed, it is shown that for 2 years following great volcanic eruptions, the surface cools significantly by 0.1° – 0.2° C in the global mean, in each hemisphere, and in the summer in the latitude bands 0° – 30° S and 0° – 30° N and by 0.3° C in the summer in the latitude band 30° – 60° N. By contrast, in the first winter after major tropical eruptions and in the second winter after major high-latitude eruptions, North America and Eurasia warm by several degrees, while northern Africa and southwestern Asia cool by more than 0.5° C.

Because several large eruptions occurred at the same time as ENSO events, the warming produced by the ENSO masked the volcanic cooling during the first year after the eruption. The timescale of the ENSO response is only 1 year while the volcanic response timescale is 2 years, so the cooling in the second year is evident whether the ENSO signal is removed or not.

These results, both the global cooling and Northern Hemisphere continental winter warming, agree with general circulation model calculations.

1. Introduction

Major explosive volcanic eruptions can inject large amounts of sulfur-rich gases (mainly SO_2) into the lower stratosphere (Rampino and Self 1984). These gases undergo rapid oxidation to sulfuric acid vapor, H_2SO_4 , which has a low volatility and condenses with water to form an aerosol haze. The resulting volcanic aerosols can enhance the mass of the natural, ubiquitous background sulfate layer by a factor of 100 or more. They are carried by the strong zonal winds in the lower stratosphere to circle the globe in a few weeks (Robock and Matson 1983). Later, they are transported equatorward or poleward by the mean meridional circulation and eddies to form a hemispheric or global dust veil. These aerosols stay suspended in the stratosphere for a few years, with a mean e -folding residence time of about 1 year.

Volcanic aerosols scatter incoming solar radiation to space, increasing planetary albedo and cooling the earth's surface and troposphere. They also absorb terrestrial radiation, warming the stratosphere. Downward longwave radiation from the warmer stratosphere acts to warm the surface, but, except for the winter in the polar region, this warming effect is an order of magnitude smaller than the cooling effect due to reduction of shortwave radiation (Harshvardhan 1979). A direct

calculation of the tropospheric radiative impact of the El Chichón eruption in April 1982 (Ramanathan 1988) shows that the decadal average radiative cooling may be 0.2 – 0.4 W m^{-2} , which can be compared with the 0.45 W m^{-2} total trace gases heating from 1975 to 1985. This shows that even averaged over a decade, volcanoes can be important causes of climate change as compared to anthropogenic greenhouse gases. Harshvardhan (1979) and Lacis et al. (1992) have shown the net effect of submicron volcanic aerosols to be a reduction of about 3 W m^{-2} for every 0.1 in optical depth of the aerosols. The instantaneous forcing after the 1982 El Chichón eruption or the larger 1991 Pinatubo eruption produced a cooling forcing larger than the warming forcing of all anthropogenic greenhouse gases in the atmosphere at that time. Dutton and Christy (1992) have noted the correspondence between measured reduction in incoming solar radiation and the climatic response to the Pinatubo eruption of 1991.

The spatial distribution of volcanic aerosol will, of course, affect the forcing. For both the recent El Chichón and Pinatubo eruptions, at essentially the same latitude, the distribution of aerosols in the Tropics was different the first summer. The El Chichón aerosols stayed in the latitude band from 0° – 30° N (Strong 1984), while the Pinatubo aerosols straddled the equator (McCormick and Veiga 1992; Stowe et al. 1992). After the summer, in both cases the distribution was similar, with aerosols spreading fairly uniformly in the Tropics and to both poles (Strong 1984; L. Stowe 1993, personal communication). Clearly, the volcanic forcing

Corresponding author address: Dr. Alan Robock, Department of Meteorology, University of Maryland, College Park, MD 20742-2425.
E-mail: alan@atmos.umd.edu.

depends on the location of the aerosols, but in earlier cases, this distribution is unknown.

The effect of volcanic aerosols on climate has been studied in the past both by examining past records and with climate models (Robock 1991). Because large volcanic eruptions are relatively rare and El Niño/Southern Oscillation (ENSO) events sometimes occur simultaneously and mask the volcanic signal, most of the past observational studies had problems identifying a clear volcanic signal. Angell (1988) and Mass and Portman (1989), however, attempted to remove the ENSO signal, and their global average and hemispheric results showed clear volcanic signals. But neither of them examined regional patterns, looked at seasonal patterns, nor used a global gridded surface temperature dataset.

In this paper, we examine the regional and seasonal patterns of surface temperature effects of large volcanic eruptions with the most comprehensive global surface temperature available. We focus on the short-term (a few years) effect of historic major volcanic eruptions, even though a long-term effect is possible, due to long-time scales of oceanic response for a few decades after the eruptions (Robock 1978, 1979; Rind et al. 1992). A recent paper (Robock and Liu 1994) analyzed regional climatic effects of volcanoes as seen in a general circulation model (GCM) simulation and we compare our observational results to these. First, we describe the data and analysis method. The following section discusses the temperature anomalies after major volcanic eruptions. Finally, discussion and conclusions are presented.

2. Data and analysis

a. Data

A global surface temperature dataset has been produced by the Climatic Research Unit of the University of East Anglia (Jones et al. 1986a,b,c; Jones 1988) and updated to include global surface air temperature observations over land and sea surface temperatures from ship observations (Houghton et al. 1990; Jones et al. 1991; Jones and Briffa 1992). We used this dataset of monthly average, gridded ($5^\circ \times 5^\circ$) surface temperatures, from January 1854 through December 1993, which was kindly provided by Phil Jones. The dataset consists of monthly average temperature anomalies with respect to the mean for the period 1951–80, the period of best data coverage. The spatial coverage of the dataset is incomplete and changes with time. Coverage in the Northern Hemisphere is always greater than the Southern Hemisphere. The data from Antarctica are available only since 1957. In this study, we use 3-month running means so as to smooth large amplitude fluctuations (e.g., the 30–60 day oscillation in the Tropics).

b. Analysis

To determine the volcanic signals in climate change, we first need to remove two principal nonvolcanic components with which we are concerned. One is low-frequency (timescale larger than 10 years) variations, which overall show a warming trend during the period of the data. The causes of these variations may include natural internal oscillations, greenhouse gases, tropospheric aerosol, periods of volcanism, or solar variations (Robock 1979) but will not be addressed in this paper. The other component is the high-frequency (timescale less than 10 years) Southern Oscillation signal.

1) LOW-FREQUENCY VARIATIONS

We use high-pass Lanczos filtering (Duchon 1979) to remove the low-frequency variations with periods longer than 10 years. Since long-term surface air temperature variations have specific seasonal and regional patterns, as seen in both model simulations and data analyses (Houghton et al. 1990), we filtered for each month and each grid point. This is important since we are searching for short-term regional signals and do not want the long-term trends to interfere. We will use only the high-frequency temperature data, calculated separately for each grid point for each month, in this paper. As a demonstration of the effects of this filtering on the global scale, Fig. 1 shows the global annual-average data, the global annual averages of the low- and high-frequency components, and the land- and ocean-average high-frequency anomalies.

2) EL NIÑO/SOUTHERN OSCILLATION SIGNAL

The Southern Oscillation (SO) is a result of complex air–sea interactions, which cause large SST variations in the tropical Pacific and interannual fluctuations in climate. It is well known that the low phase of the SO (warm event or El Niño) is associated with above-normal eastern and central Pacific sea surface temperatures, while negative SST anomalies occur in conjunction with the high phase (cold event or sometimes called La Niña). The term ENSO (El Niño/Southern Oscillation) event is usually applied to both warm and cold variations of tropical SST.

ENSOs occur at irregular intervals of 2–9 years and typically last 1 year. An ENSO is a large tropical fluctuation, and both observational studies (e.g., Horel and Wallace 1981) and theoretical concepts (e.g., Hoskins and Karoly 1981) suggest that this kind of anomalous air–sea interaction in the region of the tropical Pacific can play a major role in some extratropical behavior. ENSO makes an important contribution to high-frequency surface air temperature anomalies in some parts of the world (Halpert and Ropelewski 1992).

In recent history, some major volcanic eruptions have happened around El Niño events (Mass and Portman 1989), with the most obvious cases being

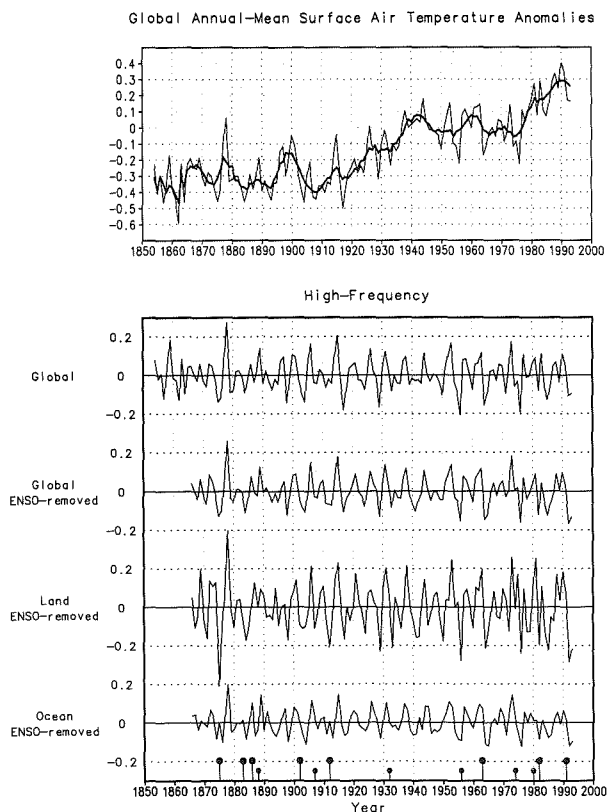


FIG. 1. The global, annual-average data and the low- and high-frequency. The top figure includes the raw and low-pass data. Across the bottom are indicated the times of the large and smaller volcanic eruptions listed in Table 1. The signal of many of these eruptions can be seen in the filtered temperatures.

Agung in 1863, El Chichón in 1882, and Pinatubo in 1991, which correspond to El Niños in 1863, 1882–83, and 1991–92. Because the climatic response to ENSO is of the same amplitude and timescale as volcanic responses, it is necessary to separate them to examine the volcanic signal. This has been attempted previously for globally and hemispherically averaged, annually averaged temperatures by Jones (1988) and applied to the search for volcanic signals by Angell (1988) and Mass and Portman (1989). In this paper, we extend the analysis to regional and seasonal patterns with a global surface temperature dataset.

The coincidence of the large April 1882 El Chichón eruption with the beginning of the largest El Niño of the century engendered much speculation about a cause and effect relationship. We do not address that issue in this paper.

The most commonly used measure of ENSO is the Southern Oscillation index (SOI), which is the difference in sea level pressure between Tahiti (18°S , 150°W) and Darwin (12°S , 131°E) (Chen 1982). The extended SOI series (Ropelewski and Jones 1987) was used to examine the relationship between ENSO and surface temperature variations (Jones and Kelly 1988;

Jones 1988). The SOI series was produced by standardizing (subtracting the mean, then dividing by the standard deviation) the Tahiti and Darwin monthly mean sea level pressures, subtracting standardized Darwin from standardized Tahiti, and then standardizing the difference. Jones and Kelly (1988) showed the strongest relationship between annual-average SOI and hemispherically averaged or globally averaged temperature was when SOI leads temperature by 6 months. Jones (1988) established a linear regression relationship between annual-mean SOI and high-frequency global temperatures and showed that ENSO explained 20%–30% of the high-frequency temperature variance and that the variance explained is similar for both negative and positive index values.

The linear relationship between SOI and temperature is not simple, however, and has specific regional and seasonal patterns, with the highest correlations at different lags in different locations. There is a nonlinear component as well for some seasons and regions, which is dependent at least on the type or strength of the event (Livezey and Mo 1987; Barnston et al. 1991). This implies that the results here must still be interpreted with caution. Additionally, the SOI is not the optimal measure of ENSO, the SST anomaly pattern. Furthermore, the SOI in the earlier part of the record is less reliable. For all these reasons it is quite possible that for certain regions or seasons the ENSO signal is misrepresented or understated. Nevertheless, due to the lack of complete theoretical understanding of extratropical ENSO effects, coupled with the small number of well-documented occurrences, either with or without simultaneous volcanic eruptions, all of which are somewhat different, we chose to use a linear relationship between SOI and surface temperatures for this study, keeping in mind that in the future it may be possible to make a more accurate representation.

Rasmusson and Carpenter (1982), who composited the El Niño events for 1950–73, described a close tie between ENSO and sea surface temperature anomalies. They showed that the warming along the west coast of South America reaches a maximum in April–June and the peak of SST anomalies in the eastern and central Pacific occurs around December. The seasonal cycle of these anomalies are clearly described in that paper. Recently, Halpert and Ropelewski (1992) studied the surface temperature patterns associated with ENSO and found consistent temperature patterns associated with the low and high phases in several separate regions, in both Tropics and extratropics, based on 100 years of past station data.

In this study, the SOI series (Ropelewski and Jones 1987), extended back to 1866, is used to establish the relationship between ENSO and surface temperature variations. We calculated the correlations between the SOI series and high-frequency surface temperature anomalies for each 3-month season (DJF, MAM, JJA, SON). ENSO explains the most

variance when SOI is simultaneous with surface temperature anomalies over the ocean and SOI leads surface air temperature anomalies over land by one season, and we used these lags for our correlation calculations. If we had different specific lags for each region, the correlations would be slightly higher, but this might induce spurious small-scale patterns as each ENSO event is not identical.

Figures 2 and 3 show the correlation between SOI and high-frequency surface temperature anomalies for the period 1866–1993 for each season. They show a

typical ENSO-related surface temperature anomaly pattern. High negative correlations (such as negative SOI and positive surface temperature anomalies during El Niño events) dominate the tropical region, both over land and ocean, except in the west Pacific, with one maximum centered in the eastern and central tropical Pacific and another in the tropical Indian Ocean. This pattern, including the “boomerang” of large positive correlations connecting the central midlatitude Pacific of both hemispheres, is similar to the pattern found over the ocean by Wright et al. (1985) and over land

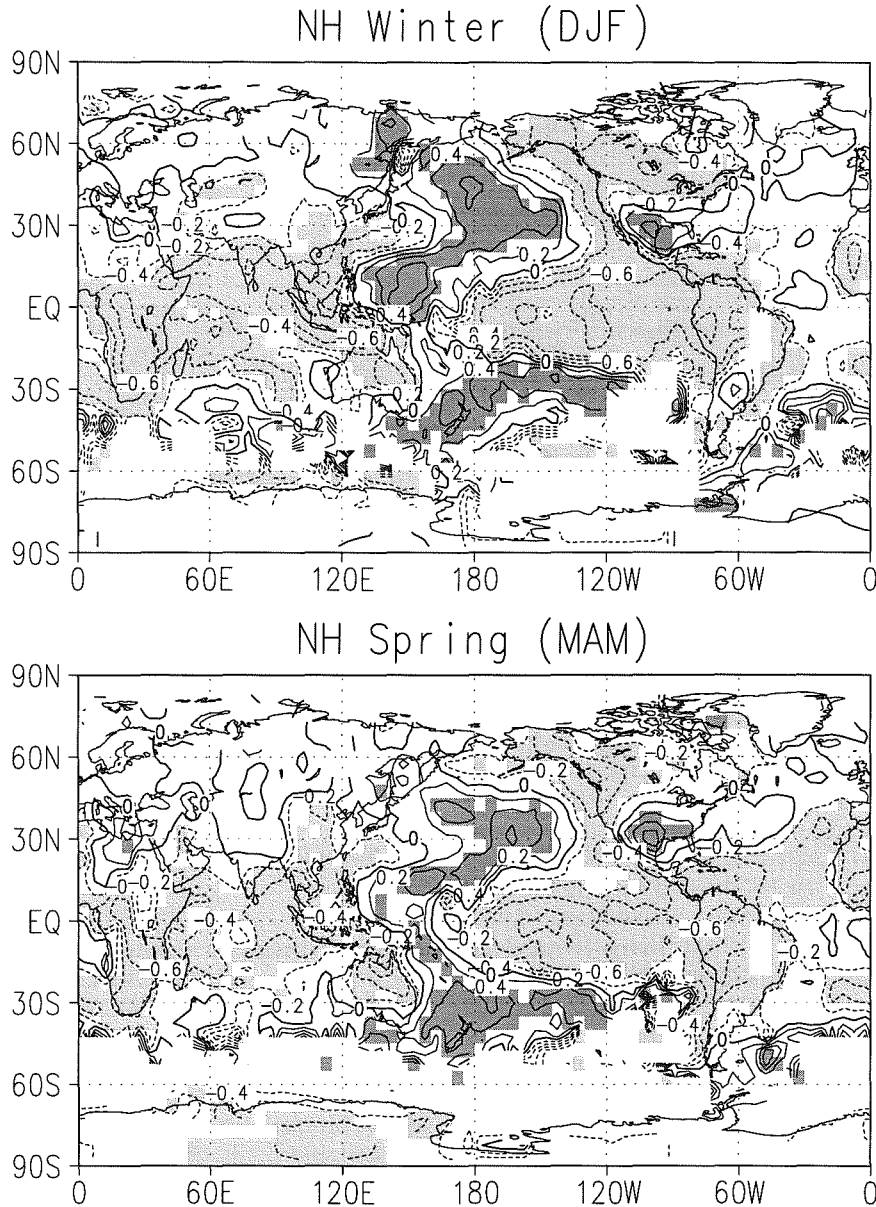


FIG. 2. Correlation between SOI and high-frequency surface temperature anomalies for the period 1866–1992 for NH winter (DJF) and NH spring (MAM), with temperature lagging SOI by one season over land and no lag over the ocean. The timing of the maps is set by the temperature time series. Correlations significant at the 5% level are shaded. Contour interval is 0.2.

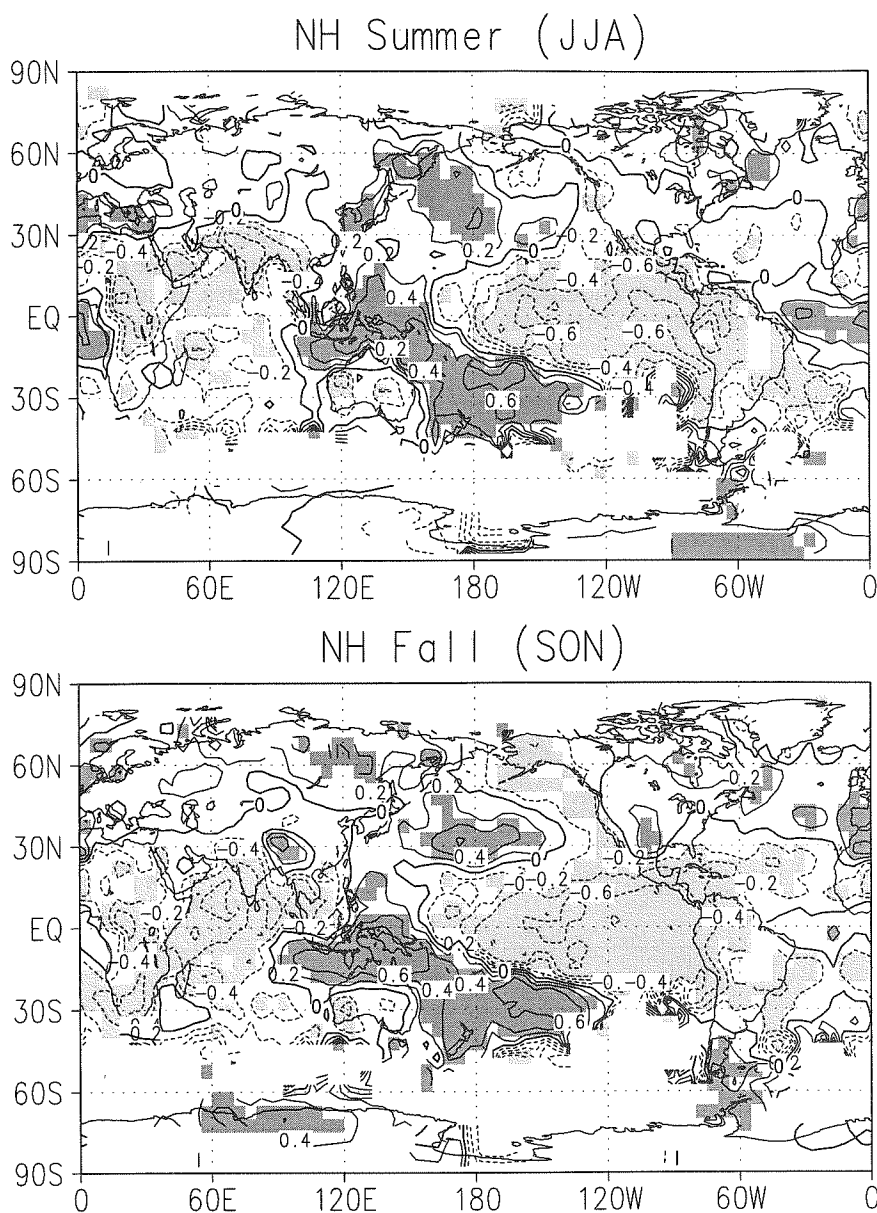


FIG. 3. Same as Fig. 2 but for NH summer (JJA) and NH fall (SON).

by Halpert and Ropelewski (1992). In the extratropics of the NH, a mixed TNH (Tropical/Northern Hemisphere: Livezey and Mo 1987) and PNA (Pacific/North America) pattern is seen, with negative correlations in north and central North America and positive correlations in southern North America and the central North Pacific, in the winter. In the spring, the pattern is weaker with the negative correlations centered on the west coast of North America. The winter pattern over Canada agrees very well with the one shown in Fig. 6 of Halpert and Ropelewski (1992). All of the patterns discussed above are statistically significant at the 5% level. Significant correlations explained 30% of

the high-frequency temperature variance in the Tropics (20°S–20°N) and 55% in the central and eastern Pacific (10°S–10°N, 160°E–80°W). In other areas, there are small correlations, which are not statistically significant.

Based on the above correlations, we established a linear regression relationship between high-frequency surface temperature anomalies (ΔT) and the SOI series for each grid point:

$$\Delta T = a + b \text{ SOI},$$

where a and b are regression coefficients calculated for the 1866–1992 period. Then, using the above relationship, we removed the ENSO signals from the high-

TABLE 1. List of the 15 largest stratospheric-aerosol-producing volcanoes since 1866; those with DVI ($d.v.i./E_{max}$) ≥ 250 or VEI ≥ 5 . Also shown are month and year of eruptions, latitude of volcano, the dust veil index ($d.v.i./E_{max}$) (Lamb 1970, 1977, 1983; Robock 1991), and volcanic explosivity index (VEI) (Simkin et al. 1981; Newhall and Self 1982; Bluth et al. 1992; S. Self 1993, personal communication). The 6 volcanoes marked with * (DVI ≥ 600 or VEI ≥ 6) were used for the preliminary analysis and those with + were added for the winter warming analysis.

Volcano	Month/year of eruption	Latitude	d.v.i./ E_{max}	VEI
Askja	March 1875	65°N	1000	5
Krakatau*	August 1883	6°S	1000	6
Tarawera+	June 1886	38°S	800	5
Bandai+	July 1888	38°N	500	4
Soufrière	May 1902	13°N	300	4
Santa Maria*	October 1902	15°N	600	6
Ksudach+	March 1907	52°N	500	5
Katmai (Novarupta)*	June 1912	58°N	500	6
Quizapo (Cerro Azul)+	April 1932	36°S	70	5
Bezmyianny+	March 1956	56°N	30	5
Agung*	March 1963	8°S	800	4
Fuego+	October 1974	14°N	250	4
Mt. St. Helens	May 1980	46°N	500	5
El Chichón*	April 1982	17°N	800	5
Mt. Pinatubo*	June 1991	15°N	1000	6

frequency surface temperature variations. Because the ENSO-related patterns differ from case to case and are not related to temperature in a simple linear way, it is impossible to remove the ENSO signal completely by this statistical method. For the globally averaged annual-average data, Fig. 1 also shows the effects of this procedure.

Livezey and Mo (1987) and Barnston et al. (1991) both point out that there are different patterns of response over North America in winter to different ENSO events, but that we do not know how to identify which pattern will occur for which ENSO. We also note that Kirchner and Graf (1994), with GCM simulations, find distinct patterns of response to volcanic and ENSO forcing in winter. The main ENSO signal is a warming in the Tropics, which can be removed well by our procedure.

3. Choice of volcanoes

It has become clear in the last decade (e.g., Rampino and Self 1984) that the effect of a volcano on climate is most directly related to the sulfur content of emissions that reach into the stratosphere and not directly to the explosivity of the eruption, although the two are highly correlated, the 1980 Mount Saint Helens eruption notwithstanding. These sulfur gases convert to small sulfate particles, which persist for several years in the stratosphere and efficiently scatter the incoming sunlight, reducing the direct and total solar radiation reaching the ground. This volcanic dust veil also absorbs longwave and shortwave radiation,

heating the stratosphere and producing anomalous stratospheric circulation when there is a gradient in the heating.

To investigate the effects of volcanic eruptions on climate, it would be desirable to have a volcanic index that is proportional to the physical effect of the volcanic dust veil on climate, namely, the net radiation deficit, or the mass loading. If the index is incomplete in its geographical or temporal coverage, if it assumes that surface air temperature drops after an eruption and uses this information to create the index, or if it is a measure of some property of volcanic eruptions other than its long-term stratospheric dust loading, it will be unsuitable for this type of study. All volcanic indices produced so far suffer from one or more of these problems. Yet, if the deficiencies of each index are kept in mind, they can be used cautiously.

The relative merits and deficiencies of the available indices are discussed in detail by Robock (1991). The two classic indices that have been used in many past studies are the dust veil index ($d.v.i.$) of Lamb (1970, 1977, 1983), and its modifications by Mitchell (1970), and the volcanic explosivity index (VEI) of Simkin et al. (1981) and Newhall and Self (1982).

The formula for the $d.v.i.$ includes a term E_{max} , which gives an estimate of the fraction of the globe covered by the dust veil. To compare the amount of material emitted from volcanoes, it is convenient to present $DVI = d.v.i./E_{max}$. As discussed by Robock (1978, 1981a), the Mitchell volcanic compilation for the NH is more detailed than Lamb's, because Lamb excluded all volcanoes with $DVI < 100$ in producing his NH annual-average DVI [Lamb 1970: Table 7(a), p. 526].

Lamb's DVI has been often criticized (e.g., Bradley 1988) as having used climatic information in its derivation, thereby resulting in circular reasoning if the DVI is used as an index to compare to temperature changes. In fact, for only a few eruptions between 1763 and 1882 was the NH-averaged DVI calculated based solely on temperature information, and these values do not affect the analysis in this paper. Robock (1981a) created a modified version of Lamb's DVI, which excluded temperature information. When used to force a climate model, the results did not differ significantly from those using Lamb's original DVI, demonstrating that this is not a serious problem.

The VEI has also been criticized as an index of explosivity and not of stratospheric loading, with the 1980 Mt. Saint Helens eruption as an example of a very explosive eruption (VEI = 5) without a large stratospheric injection. In spite of this example, a recent study by Robock and Free (1995) has shown that the DVI and VEI, when taken as 10 to the power VEI (Schönwiese 1988), as well as newer compilations by Khmelevtsov et al. (1995) and Sato et al. (1993), are all highly correlated and all indicate the same large vol-

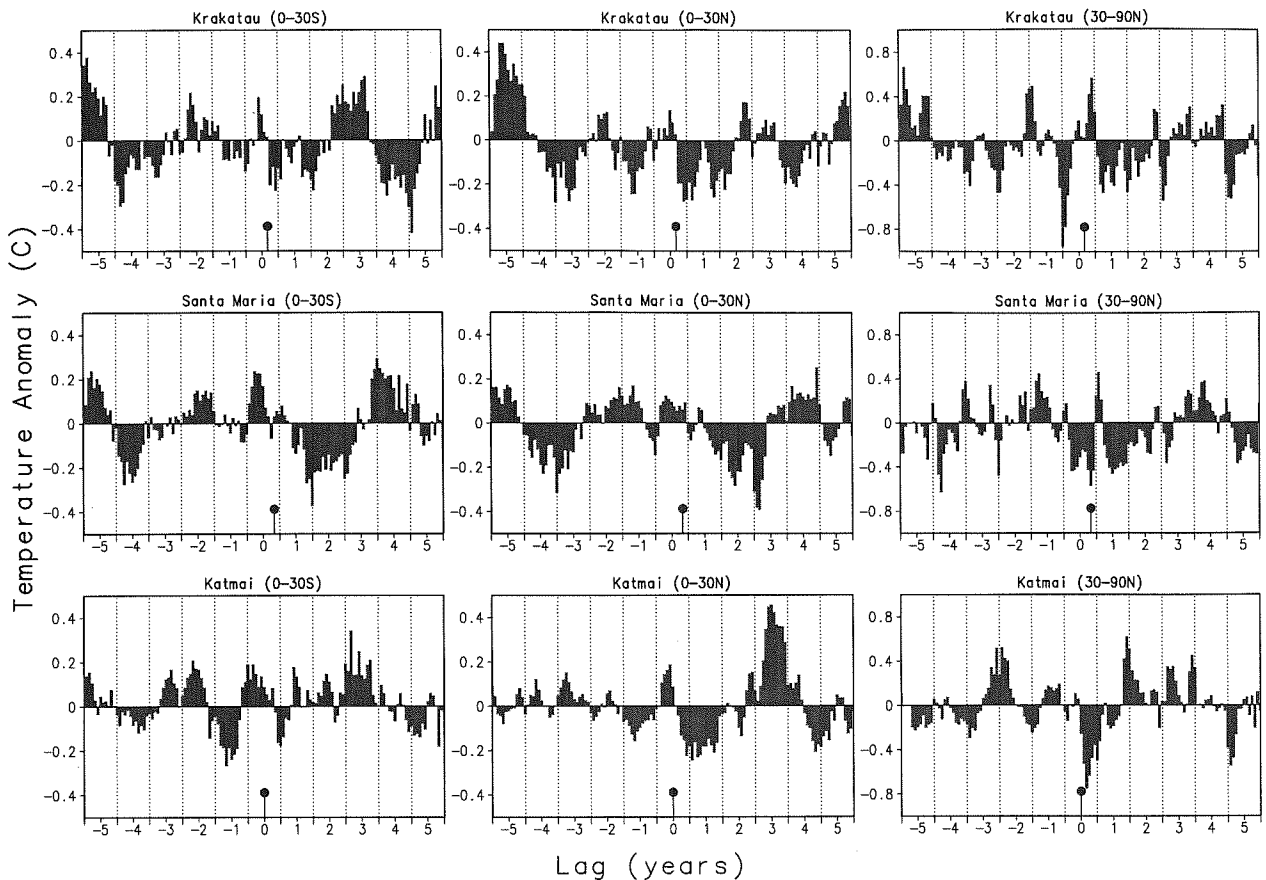


FIG. 4. Latitude band anomalies for Krakatau, Santa Maria, and Katmai, all plotted with respect to the mean for the 5-year period before the volcano. Year 0 is the year of the eruption, and the precise time of the eruption is indicated at the bottom of each graph. The years are labeled at the center of each year; vertical dotted lines are drawn for January of each year. The latitude band 30° – 90° S is not shown as the temperature data are too sparse.

canoes. Although the VEI is clearly an imperfect measure of climatically important volcanoes, it does indicate the largest ones.

Table 1 gives a list of all the volcanoes since 1866 with $DVI \geq 250$ or $VEI \geq 5$. For this study then, we wanted to take the largest volcanoes of the period for which we have temperature data but wanted them separated by at least 5 years. The criteria we chose were rather arbitrary, but the results do not depend crucially on this choice as there were enough volcanoes with a large impact to outweigh the addition or omission of one or two other volcanoes. We decided on the criteria of $DVI \geq 600$ or $VEI \geq 6$ to use for our preliminary analysis.

The six volcanoes chosen for our preliminary analysis are indicated in Table 1. Although meeting our criteria, we excluded Askja because the global distribution of temperature data was too sparse before 1880 and Tarawera because it was within 5 years of a larger volcano (Krakatau). All of these six volcanoes are tropical, with exception of Katmai.

4. Volcanic signals in surface temperature variations

a. Global and zonal averages

In Fig. 1, for the high-pass, annual-average data with ENSO removed, we can see the signal of cooling for a few years after some of the eruptions fairly clearly, especially over the oceans. This is surprising, as conventional wisdom holds that short-term signals in the climate system such as this should become evident first over land, which has a lower thermal inertia. However, the temperature changes we are examining, anomalies of less than 1°C , are much smaller even than the seasonal cycle of the tropical oceans and so can easily occur in the ocean. The higher sensitivity of land, if it is relevant in this case, also allows the land to respond to all other forcings more rapidly, so the problem becomes one of signal versus noise and of the relative strength of the forcings as functions of latitude.

The approach of comparing temperature changes with times of specific volcanic eruptions, and pointing out that the apparent signal is suggestive of cause and

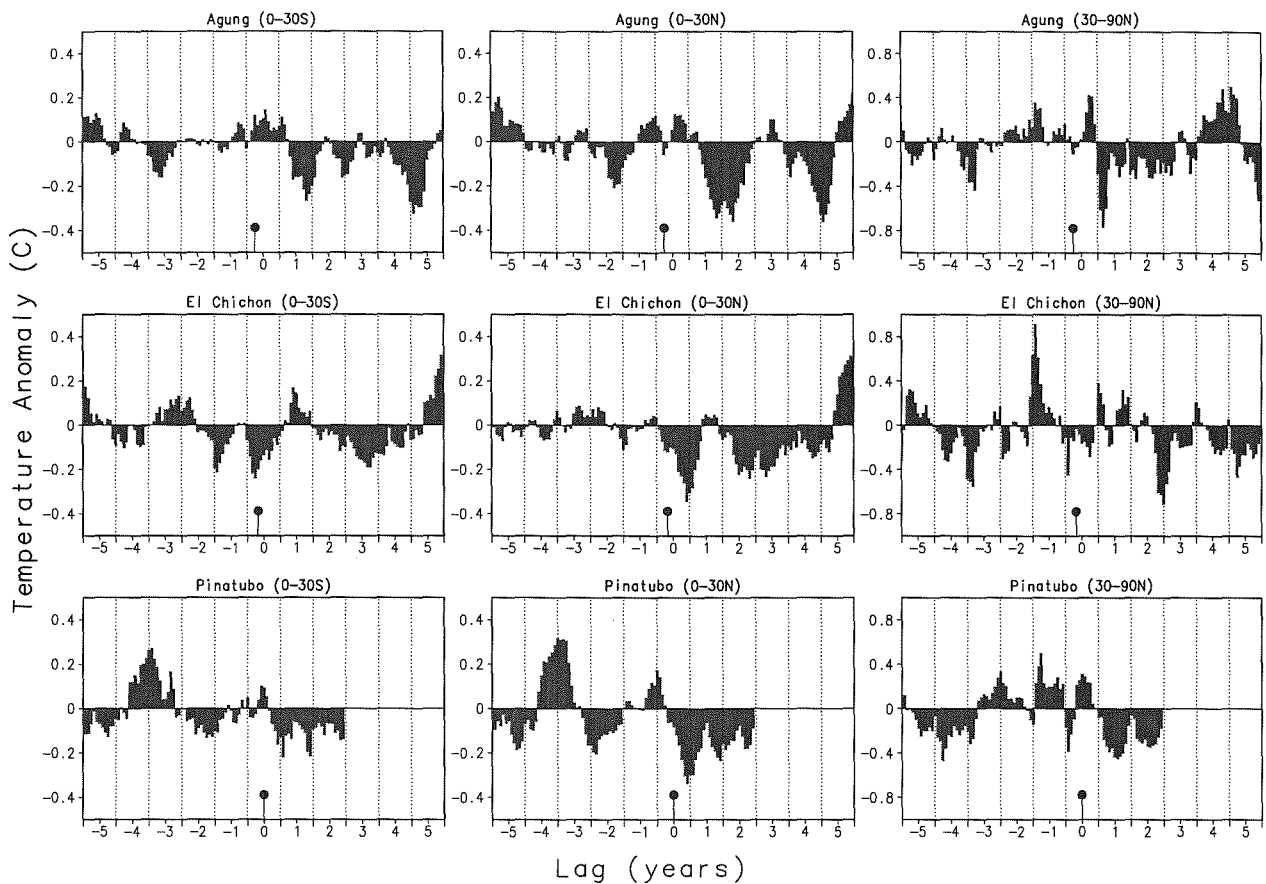


FIG. 5. Same as Fig. 4 for Agung, El Chichón, and Pinatubo.

effect, has been used by a number of investigators in the past, including Humphreys (1940), Yamamoto et al. (1975), Angell and Korshover (1985), Kondo (1988), Angell (1988), and Xu (1988). But this approach does not give a quantitative measure of the impact of a typical volcano. To further examine this impact, we choose to perform a superposed-epoch analysis, first used by Mitchell (1961) to look at the effects of volcanoes on climate and used by many investigators since (Robock 1991).

By using the volcanoes indicated in Table 1, we calculated for each volcano the mean of the temperature for each month for each grid point for the 5 years prior to the year of the eruption and then examined the latitude band, monthly average anomalies with respect to this mean for the period starting 5 years before each eruption to 5 years after each eruption. The anomalies thus generated are presented in Figs. 4 and 5 for each volcano.

We expected to see a clear large volcanic cooling signal in the high latitudes in winter, due to the sea ice/thermal inertia feedback (Robock 1981b, 1983, 1984a, 1984b). We found, however, that the volcanic cooling signal was more clearly seen in the Tropics and

subtropics, especially in the NH, and that in the winter in the NH high latitudes there is actually a relative warming beginning in the winter following the eruption. The only exception is Katmai, at 52°N . For this case (Fig. 4), the largest response is a cooling at 30° – 90°N , in the same latitude band as the volcano, which lasts through the first winter, although the winter is not as cool as the summer. The following winter this same latitude band is warmer than normal. It is possible that the signatures of Tarawera (1886) and Awu (1966; DVI = 200, VEI = 4) are seen after Krakatau and Agung, respectively, in years 4 and 5. Although the sea ice/thermal inertia feedback amplifies the climatic signal in high latitudes in equilibrium calculations with energy-balance models and GCMs, the natural variability is also much larger in high latitudes. Furthermore, the winter warming signal we have discovered (Robock and Mao 1992; also see below), a nonlinear dynamical effect that would not be seen in the previous energy-balance simulations of volcanic effects, cancels out the cooling necessary to produce the sea ice/thermal inertia feedback in the first winter after the eruption. Even in the winter, the net radiative forcing from a volcanic aerosol layer is cooling at latitudes south of 65°N with

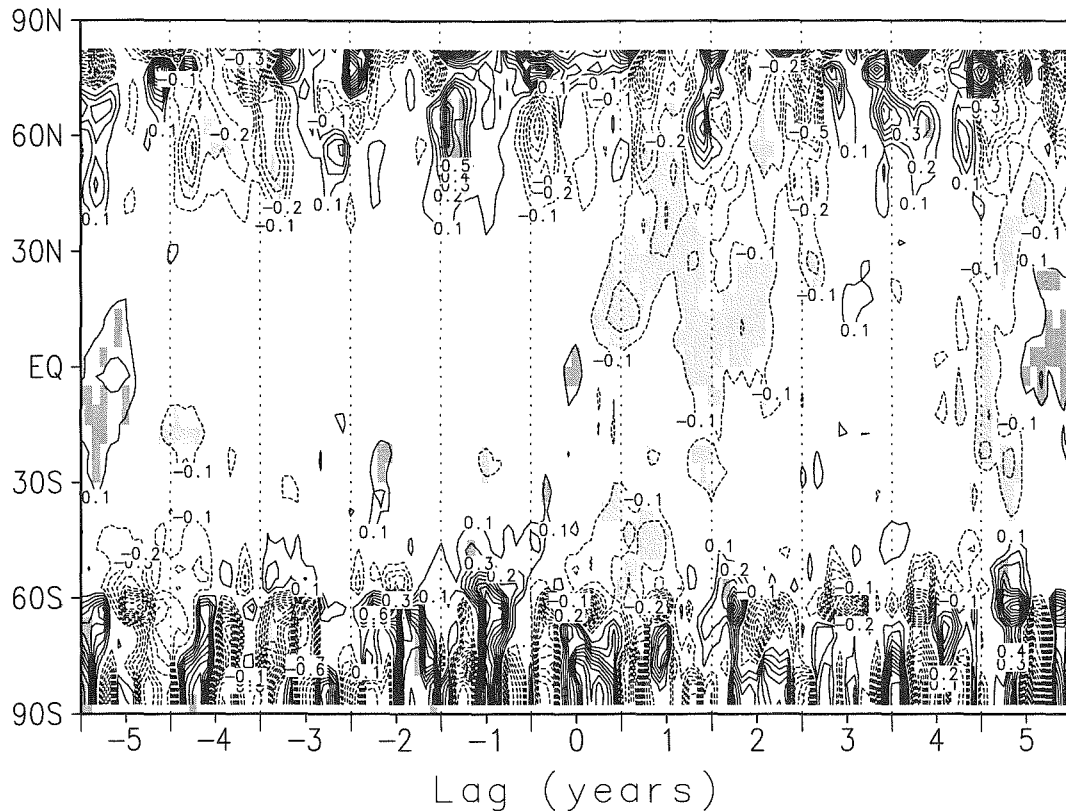


FIG. 6. Average of the six cases in Figs. 4–5. Contours are every 0.1°C , with the 0°C contour omitted. Light shading indicates cooling significant at the 5% level, and darker shading indicates warming significant at the 5% level.

a very small warming north of there (Harshvardhan 1979), so the results shown here in the winter are dominated by dynamics, not radiation.

Although it looks like there are volcanic signals in Figs. 4 and 5, the temperature variations are quite noisy. Therefore, we performed a superposed-epoch analysis, and the results are presented in Fig. 6. A broad area of significant cooling is found in the Tropics for 2 years after the eruptions and in the NH subtropics and midlatitudes in the summer of the year following the eruptions. The shaded significant cooling region follows the location of maximum solar intensity, as would be expected if the signal is caused by reduction of insolation by volcanic aerosols. The fifth year also shows some tropical cooling, possibly the signals of Tarawera and Awu as discussed earlier. Small areas of warming are found in the NH winter centered around 50° – 60°N in the winter after the volcanoes and the next winter. Although not significant in this analysis, this winter warming signal is shown more clearly by modifying the analysis later.

We conducted our significance tests for the zonal-mean anomalies in Fig. 6 and area-averaged anomalies in Fig. 7 for each month by separating the anomalies in the whole period (1866–1993) into two groups: composite volcanic group from the six cases and non-

volcanic group, which excludes the data in the 3 years following each eruption (e.g., for El Chichón the data from April 1982 to April 1985 are not included). We processed the nonvolcanic group by removing the mean from the previous 5 years for each case, but since the mean is close to 0, it made little difference. Therefore, for our tests, we simply used the high-pass ENSO-removed data for the nonvolcanic years. Then we used a Student's *t*-test to test whether the means and variances from the two groups are significantly different from each other at 5% confidence level.

To further refine the volcanic signal, we performed averages of the data shown in Fig. 6 across various latitude bands, and these are shown in Fig. 7. In the global mean, the cooling from the middle of year 0 to the middle of year 2 is clearly seen, as well as a cooling in the first half of year 5, as discussed above. The dashed line without dots shows the results of the same analysis without first removing the ENSO signal and shows that the cooling from the middle of year 0 to the middle of year 1 is masked by the ENSO warming but the subsequent cooling is not. This separation of timescales of response, with the typical ENSO warming lasting less than 1 year but the typical volcanic cooling lasting 2 years, allows a clear attribution of the causes.

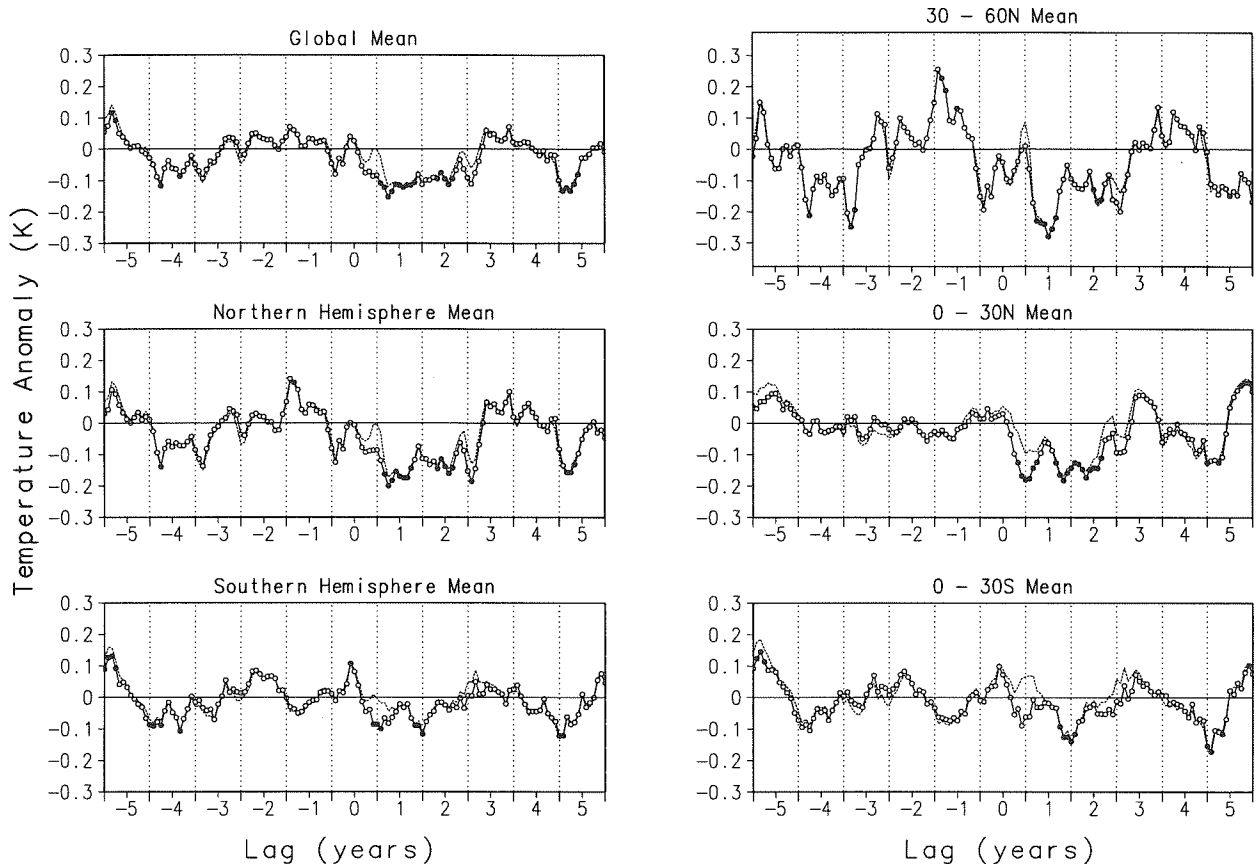


FIG. 7. Averages of the data in Fig. 6 across various latitude bands. The points that are significantly different from 0 are shaded. The dashed line without the dots is the same analysis, without removing ENSO.

The NH pattern looks similar to the global one, as it is the main contributor to the global signal due to more areas with missing data in the SH. However, it is clear that the times of significant cooling in the NH, as indicated by the solid dots, are in the summer of years 1 and 2, when reduction of solar insolation would be most effective. Similarly, in the SH, although the temperature reductions are smaller, the times of cooling are again in the summers of the first 2 years. Without removing ENSO, the cooling in the first summer would be completely missed.

The volcanic signal is seen most clearly by dividing the world into latitude bands. The bands with the most complete data are shown on the right side of Fig. 7. The NH midlatitude band (30° – 60° N) shows cooling in the summers of years 1 and 2. A clear 2-year cooling is seen in the NH Tropics (0° – 30° N). The SH tropical (0° – 30° S) signal is weaker, being significant only in the second summer at the end of year 1. Because this band has less land, it would be expected to show a smaller signal.

b. Spatial patterns

To also see longitudinal patterns of the temperature response, we plotted seasonal-averaged maps for each

season following the eruptions. We show here only the winter and summer patterns, both with and without removing the ENSO signal. These seasons correspond to the strongest signals seen in Figs. 4–7.

Winter. Figure 8 shows the NH winter temperature anomaly pattern for the six volcanoes for each of the three winters following the eruptions using the high-pass data before removing ENSO, and Fig. 9 shows the same thing after the ENSO removal. It is clear that the only pattern that changes with the ENSO removal is in the first winter (year 0–1) over the ENSO region itself in the tropical eastern Pacific Ocean, over southern Africa and bits of the Eastern Hemisphere Tropics, and over northwest and central North America. After ENSO removal, substantial warm anomalies are still seen over Eurasia, with cool anomalies over northern Africa, the Mideast, southern Asia, and Australia. Over North America, a residual of the strong pattern remains over the eastern United States.

Our hypothesis is that the warm anomalies are produced by an enhanced polar vortex, which stimulates a wave response in the winter circulation with a pattern of warm advection that prevents as much cooling as in nonvolcanic years. This enhanced vortex is caused

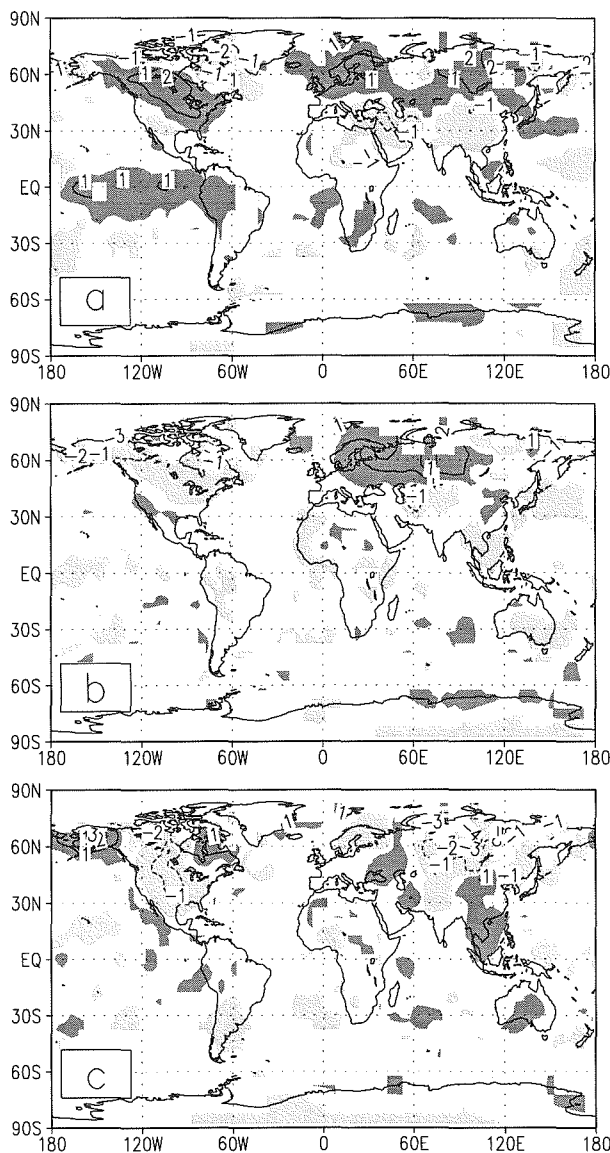


FIG. 8. (a) Map of temperature anomalies for the NH winter following the eruptions averaged for all six volcanoes, without first removing the ENSO signal. Areas with anomalies $< -0.25^{\circ}\text{C}$ are shaded and areas with anomalies $> +0.25^{\circ}\text{C}$ are shaded darkly. Contours are drawn with an interval of 1°C , with the 0°C contour not shown. (b) Same as (a) but for the second winter. (c) Same as (a) but for the third winter.

by the temperature gradient set up by the heating of the tropical stratosphere by absorption of longwave radiation by the volcanic aerosols. This was demonstrated in a preliminary study by us (Robock and Mao 1992), in GCM experiments by Graf et al. (1993), and in observational and GCM studies by Kodera (1993), who provided a theoretical framework for the dynamical response. The cooling in the subtropics is a direct radiative effect, with the largest response over Africa and Asia, the largest landmass at these latitudes.

The winter patterns in Figs. 8b–c and 9b–c for the second and third winters are also interesting. The second winter shows continued warming over Europe but cooling over North America, and the third winter shows cooling over both North America and Eurasia, as we previously expected (Robock 1984a). Perhaps after the winter dynamical response is over, the sea ice/thermal inertia feedback can operate, but sea-ice data would be necessary to verify this, and such data are sparse for more than a few eruptions.

None of the patterns in Figs. 8 and 9 exhibit field significance at the 5% level, due to the large interannual variance of winter continental temperatures. Still, on theoretical grounds, we believed that the patterns were

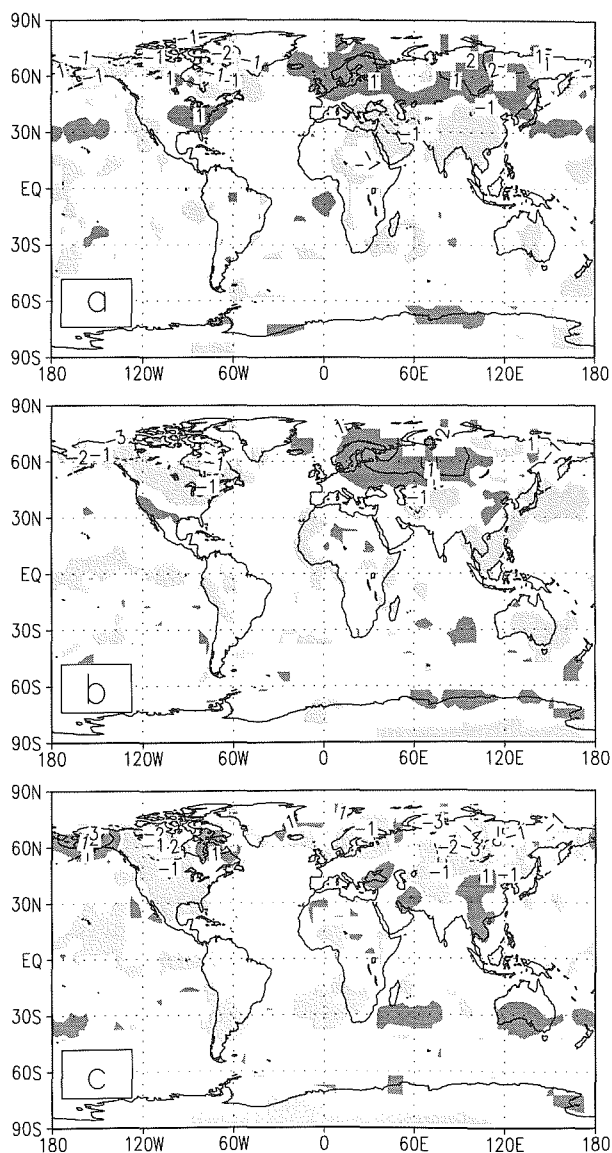


FIG. 9. Same as Fig. 8 but ENSO signal was removed first.

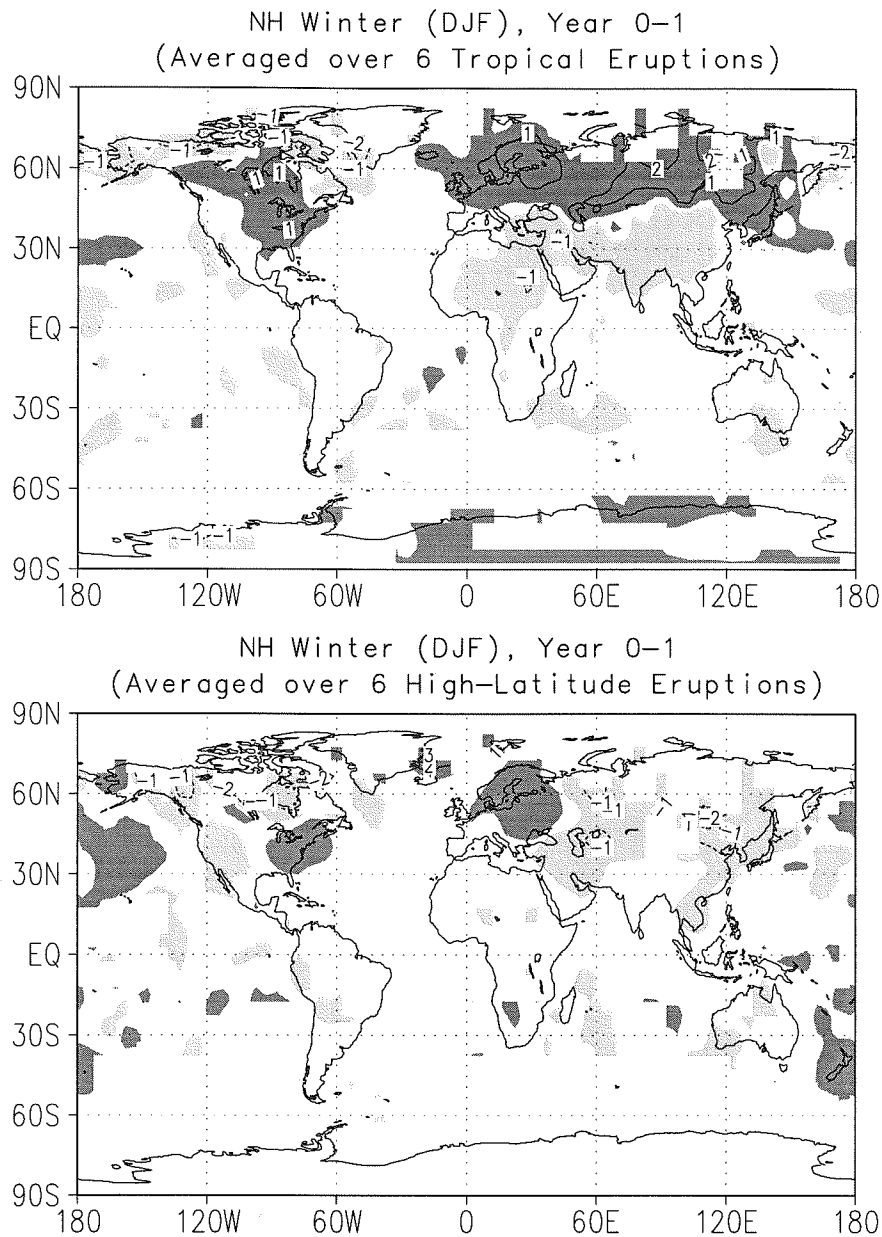


FIG. 10. Northern Hemisphere winter anomaly patterns for the first winter after the eruptions (year 0-1), after first removing the ENSO signal, for the six tropical eruptions and six high-latitude eruptions indicated in Table 1. As in Figs. 8 and 9, areas with anomalies $< -0.25^{\circ}\text{C}$ are shaded lightly and areas with anomalies $> +0.25^{\circ}\text{C}$ are shaded darkly. Contours are drawn with an interval of 1°C , with the 0°C contour not shown.

robust and so conducted further analysis to isolate a significant volcanic winter warming signal.

Our six large volcanoes contain five tropical eruptions and one large high-latitude one (Katmai). Because the stratospheric aerosol layer from high-latitude ($|\phi| > 30^{\circ}$) volcanoes does not immediately reach the Tropics and, typically, only mixes to other latitude bands when the stratospheric circulation shifts in the fall and spring, we decided to separate the winter signals

from tropical and high-latitude eruptions by examining the first winter after tropical eruptions but waiting until the second winter following high-latitude eruptions to give the aerosols time to reach the Tropics and produce this effect. To further refine the NH winter warming signal, we were only interested in the year or two following the volcanoes, so relaxed the 5-year rule and added Tarawera and five more volcanoes that were not quite strong enough to meet the criteria for the previous

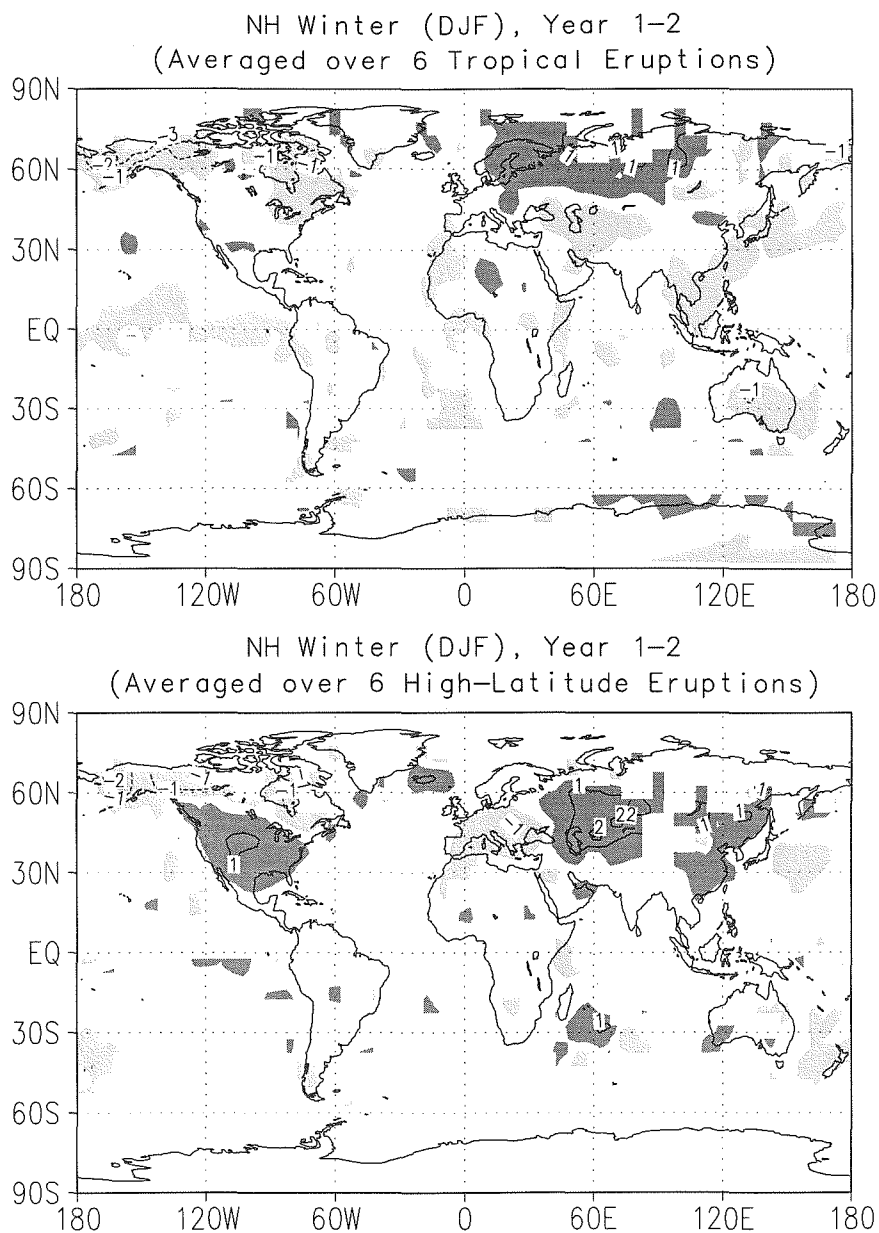


FIG. 11. Same as Fig. 10 but for the second winter (year 1-2).

analysis (Table 1). We did not use the 1980 Mt. Saint Helens eruption because it had a small stratospheric SO_2 input as most of the blast was lateral (Robock 1981b).

Figure 10 shows the winter patterns, after first removing the ENSO signal, for the first winter for these 12 volcanoes, with the patterns for the six tropical eruptions and six high-latitude eruptions shown separately, and Fig. 11 shows the patterns for the second winter. The winter warming signal over both North America and Eurasia now appears much more clearly in year 0-1 for the tropical eruptions and year 1-2 for the high-latitude eruptions. The pattern previously

shown in Figs. 8 and 9 for the first winter was a mixture of the cooling from Katmai with the warming from the tropical volcanoes. For the high-latitude volcanoes, the first winter shows cooling as the radiative effects overwhelm the signal, and the dynamical effect is not strong as the aerosols have not reached the Tropics in large enough concentrations.

The persistence of the winter warming pattern over Eurasia for the first *and* second winters after the six largest eruptions (Figs. 9a,b) or after the six tropical eruptions (Figs. 10a and 11a) suggests that this is a real phenomenon. It also verifies the analysis of Groisman (1992) who examined 2-year or 3-year average

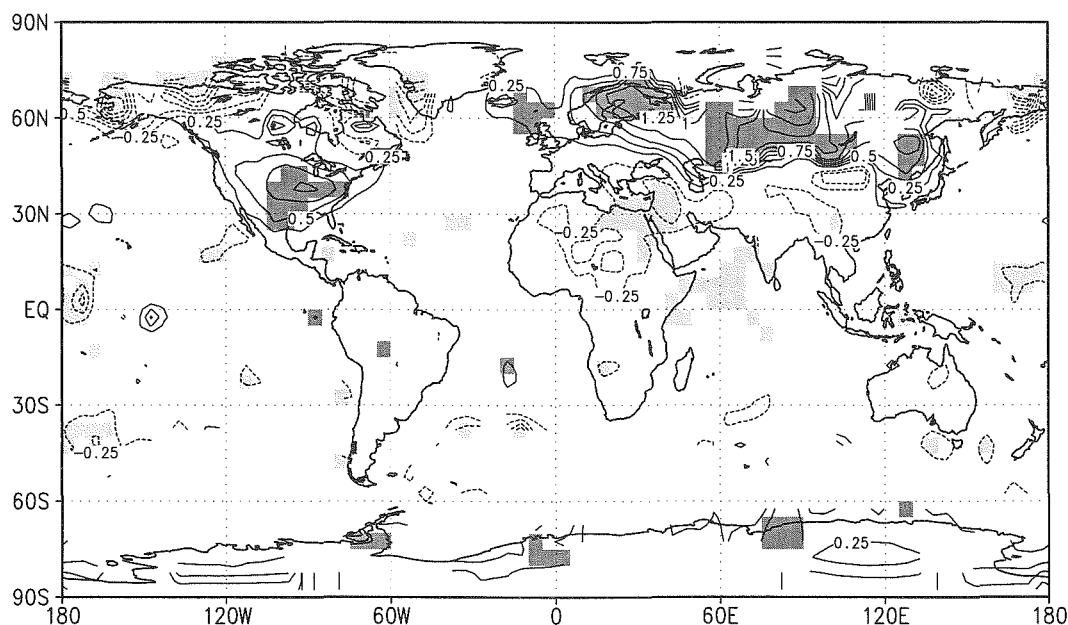


FIG. 12. Northern Hemisphere winter-average anomalies of surface temperature for the first winter after tropical eruptions and the second winter after high-latitude eruptions for the 12 eruptions indicated in Table 1. Areas with negative anomalies significant at the 5% level are shaded lightly and areas with significant positive anomalies are shaded darkly. Contours are drawn with an interval of 0.25°C, with the 0°C contour not shown.

patterns of warming over Eurasia after large eruptions because of the persistence of the winter warming.

By combining the year 0–1 signal for the tropical eruptions with the year 1–2 signal from the high-latitude ones, we show in Fig. 12 the clear winter warming signal, which is significant over North America and Eurasia for the warming and over northwestern North America, Africa, and the Middle East for the cooling. This pattern is slightly different from the one in Robock and Mao (1992) because here we removed the ENSO signal season by season. There is a bit of an a posteriori aspect to this because we did this compositing after seeing the means of the patterns, but we looked for winter warming in the second year after high-latitude eruptions on theoretical grounds.

Although it appears that the patterns in Fig. 12 over both North America and Eurasia are significant, it is still possible that a large area could have anomalies significantly different from the mean for the nonvolcanic years by chance. Therefore, we tested the field significance of the patterns over land in both continents using a permutation technique (Zwiers 1987). As illustrated in Fig. 13, for all land grid points over North America (25°–75°N, 60°–180°W) and Eurasia (25°–75°N, 0°–120°E), we conducted a Monte Carlo test of the percentage of area expected to be covered by grid points significantly different from 0 by chance. For the 127 winters in our dataset (1866–1993), we picked 12 winters at random 1000 different times and used a local Student *t*-test to calculate the percentage of area with temperature anomalies significantly dif-

ferent from the years not chosen. As was done by Livezey and Chen (1983), we plotted for each case the percentage of cases versus percentage of area that was significant in Fig. 13. The cases with the highest 5% of the area are shaded darker. We then compared the percentage of significant area in each of our regions (20.4% for North America and 25.6% for Eurasia) to the results of the permutation test and found, in both cases, that this much significant area would occur less than 5% of the time by chance. Therefore, we concluded that the patterns over both North America and Eurasia were field significant.

Figure 14 shows the ENSO-removed signal for the NH summers of years 1 and 2. Virtually all of the continental regions have cold anomalies, with the largest cooling over Asia and northern North America for year 1, but a weaker signal in year 2.

5. Discussion and conclusions

Based on the analyses of more than 100 years of land, air, and sea surface temperature records, it is shown that the major explosive volcanic eruptions produce clear temperature effects in different seasons and locations. These effects, generally, are cooling but include a winter warming signal in high-latitude NH continents. The winter warming pattern over Northern Hemisphere continents agrees well with the GCM calculations of Graf et al. (1993) and Kirchner and Graf (1995). The identifiable signals last approximately 2 years, which is shorter than previous energy-balance

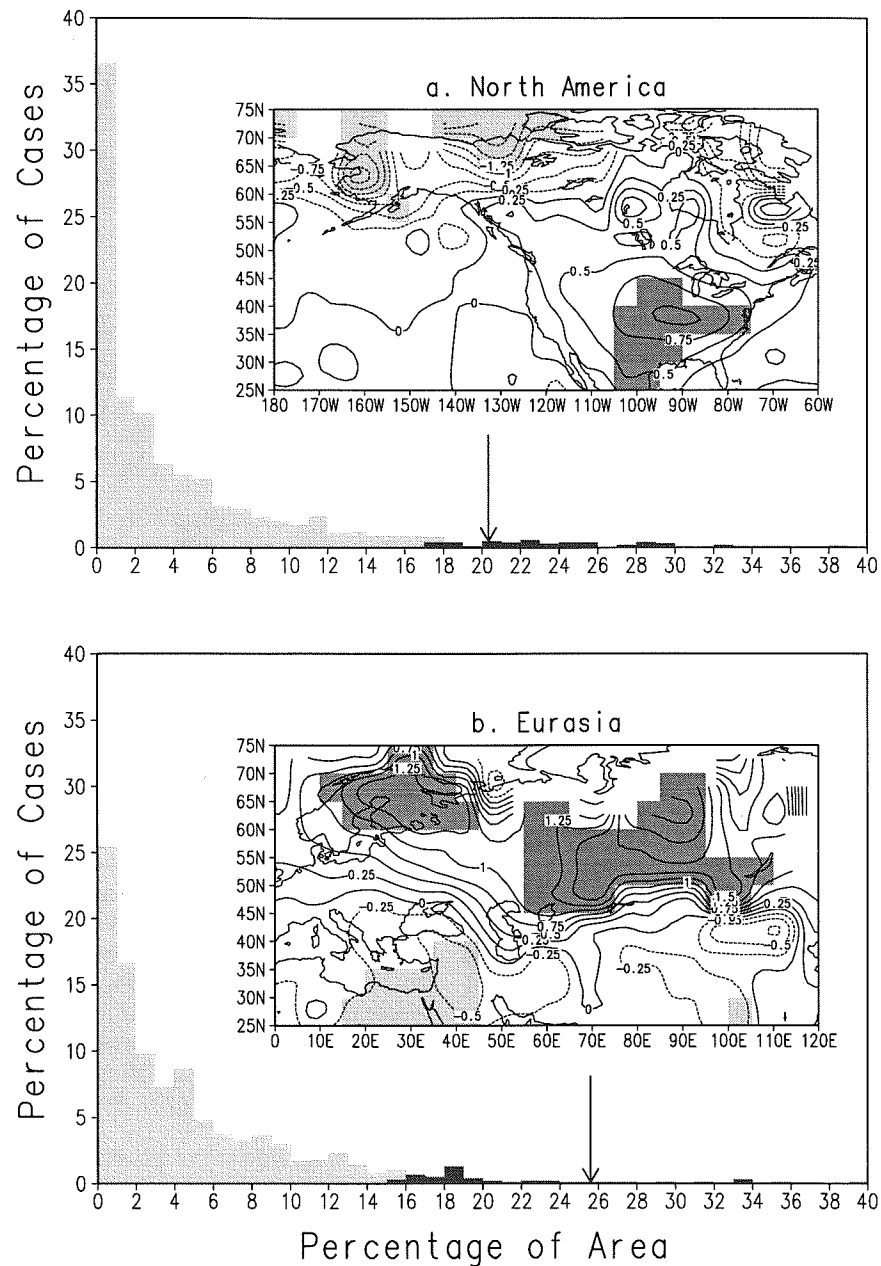


FIG. 13. Results of the field significance permutation tests described in the text for the areas shown from Fig. 12. For the land grid points over North America and Eurasia, the percentage of cases with an area significant at the 5% level is shown for 1000 cases of the average of 12 random years. The bars for the 5% of the cases with the largest area are darkly shaded. The arrows show the percentage of area significant for the regions shown. In both cases, regions are field significant at the 5% level.

(Robock 1981b, 1984b) or GCM (Hansen et al., 1988; Robock and Liu 1994) climate model simulations. Apparently, the real climate system includes more variability than these model simulations, which masks the volcanic signal after it decays to a certain small size. The summer patterns found here, of enhanced cooling over the continents, also agree with the GCM

results of Robock and Liu (1994), but the smaller-scale details (on the 1000-km scale) are different between our observations and the models, pointing out the need for more volcanic cases and more modeling studies.

It is important to separate the ENSO signal from the volcanic one and remove it to more clearly see the

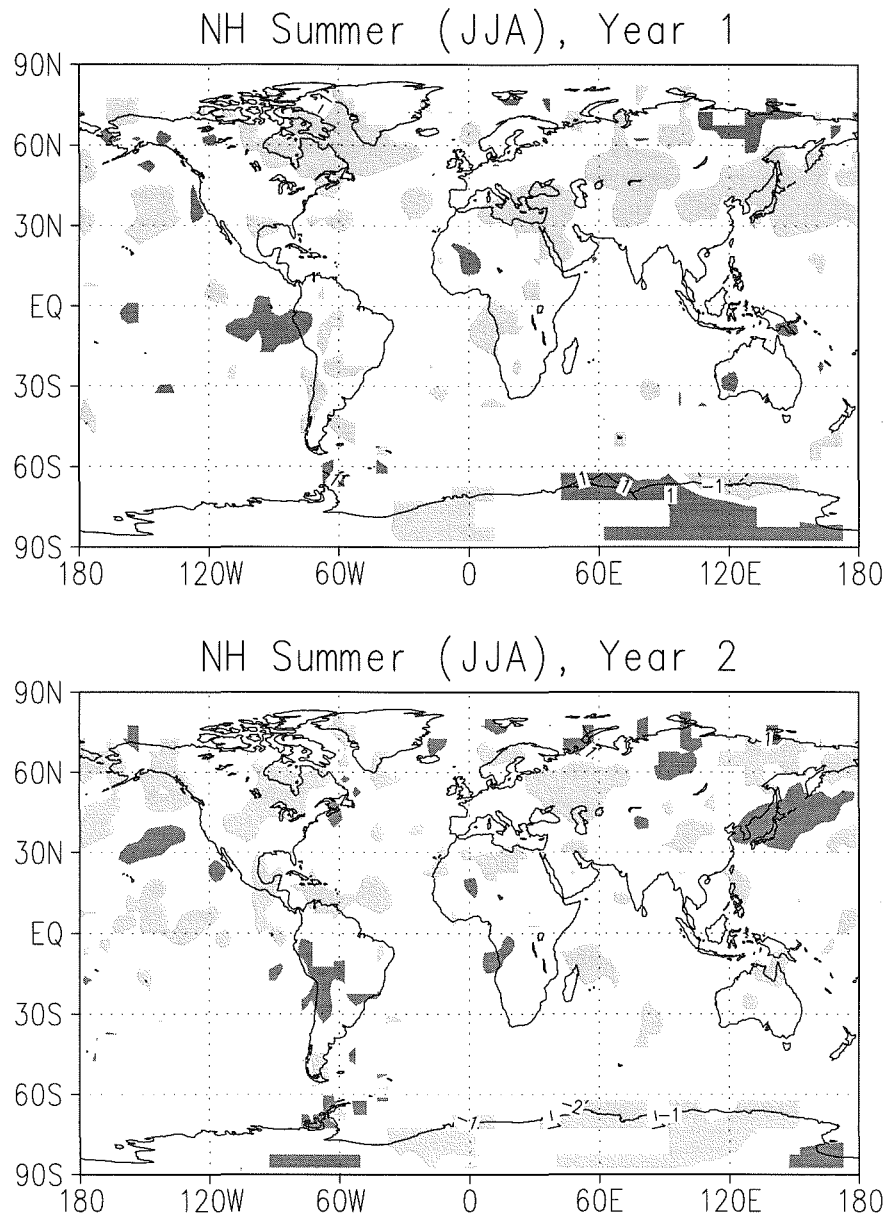


FIG. 14. Same as Fig. 9 but for the first and second summers (years 1 and 2).

volcanic signal during the first year after the eruptions, as both have high amplitudes in the Tropics. We have attempted to do this in a linear fashion, but clearly more work is required to improve this separation, in particular over North America. It is still not sure how much of the winter warming over North America is volcanic and how much is due to ENSO. The small number of cases with data limits robust statistical tests. The ENSO signal has a different spatial and temporal pattern than the volcanic one, however, due to different forcing mechanisms. By showing the volcanic patterns, both with and without removing ENSO, it is clear from Fig. 7 that for these particular volcanoes, ENSO only

affects the response in the year following the eruptions and that for the years before and after, the volcanic pattern is there with or without ENSO. The spatial patterns are also clear with or without removing ENSO. Whether volcanoes produce ENSO cannot be resolved by the analysis here, but clearly there are eruptions without ENSO and ENSO without eruptions, and the pattern of response to a volcano will have to include the effects of an ENSO, if one is happening.

In predicting short-term climate changes, both volcanoes and ENSO events must be considered. In the Tropics, for example, in the case of the 1982 El Chichón eruption, the huge ENSO event dominated the climate

change for the next year. Following the 1991 Pinatubo eruption, however, the effects of the large volcanic eruption competed with the ENSO and resulted in much less warming than in 1982–83 and even cooling at most latitudes by the middle of 1992 (Dutton and Christy 1992). In the winter over North America, both warm ENSO events and volcanic eruptions produce similar patterns, reinforcing each other in a nonlinear way (Kirchner and Graf 1995).

The timing of the winter warming effects shown here are dependent on the latitude of the eruption. Volcanic sulfate aerosols reach the Tropics from large volcanoes at all latitudes, and it is the tropical forcing that produces these effects. The response to radiative effects then depends on the response characteristics of the climate system, not the location of the initial injection. A high-latitude eruption, however, such as Katmai, will put so much aerosol into the high-latitude atmosphere that the direct radiative effect will be dominant in the first winter.

Several issues involving volcanoes and climate remain to be investigated, including the possible cause-and-effect relationship with ENSO and the possible long-term effects from periods of volcanism, such as the warming of the 1920s and 1930s during a period of virtually no volcanoes.

Acknowledgments. We thank Phil Jones for surface temperature and SOI data; Karl Taylor, Anandu Vernekar, Hans Graf, Yuhe Liu, and Gene Rasmusson for valuable discussions; three anonymous reviewers and Ants Leetmaa for valuable comments; Bob Livezey for valuable comments, actual editing of the text, and for suggesting the permutation test, all of which improved the paper; and Brian Doty for development and enhancements of the GrADS plotting software, which was used for all the figures. This work was supported by NSF Grant ATM 89-20590 and NASA Grant NAG 5-1835.

REFERENCES

- Angell, J. K., 1988: Impact of El Niño on the delineation of tropospheric cooling due to volcanic eruptions. *J. Geophys. Res.*, **93**, 3697–3704.
- , and J. Korshover, 1985: Surface temperature changes following the six major volcanic episodes between 1780 and 1980. *J. Climate Appl. Meteor.*, **24**, 937–951.
- Barnston, A. G., R. E. Livezey, and M. S. Halpert, 1991: Modulation of Southern Oscillation-Northern Hemisphere mid-winter climate relationships by the QBO. *J. Climate*, **4**, 203–217.
- Bluth, G. J. S., S. D. Doiron, C. C. Schnetzler, A. J. Krueger, and L. S. Walter, 1992: Global tracking of the SO₂ clouds from the June, 1991 Mount Pinatubo eruptions. *Geophys. Res. Lett.*, **19**, 151–154.
- Bradley, R. S., 1988: The explosive volcanic eruption signal in Northern Hemisphere continental temperature records. *Clim. Change*, **12**, 221–243.
- Chen, W. Y., 1982: Assessment of Southern Oscillation sea level pressure indices. *Mon. Wea. Rev.*, **110**, 800–807.
- Duchon, C. E., 1979: Lanczos filtering in one and two dimensions. *J. Appl. Meteor.*, **18**, 1016–1022.
- Dutton, E. G., and J. R. Christy, 1992: Solar radiative forcing at selected locations and evidence for global lower tropospheric cooling following the eruptions of El Chichón and Pinatubo. *Geophys. Res. Lett.*, **19**, 2313–2316.
- Graf, H.-F., I. Kirchner, A. Robock, and I. Schult, 1993: Pinatubo eruption winter climate effects: Model versus observations. *Climate Dyn.*, **9**, 81–93.
- Groisman, P. Ya., 1992: Possible regional climate consequences of the Pinatubo eruption: An empirical approach. *Geophys. Res. Lett.*, **19**, 1603–1606.
- Halpert, M. S., and C. F. Ropelewski, 1992: Surface temperature patterns associated with the Southern Oscillation. *J. Climate*, **5**, 577–593.
- Hansen, J. E., I. Fung, A. Lacis, D. Rind, S. Lebedeff, R. Ruedy, G. Russell, and P. Stone, 1988: Global climate changes as forecast by Goddard Institute for Space Studies three-dimensional model. *J. Geophys. Res.*, **93**, 9341–9364.
- Harshvardhan, 1979: Perturbations of the zonal radiation balance by a stratospheric aerosol layer. *J. Atmos. Sci.*, **36**, 1274–1285.
- Horel, J. D., and J. M. Wallace, 1981: Planetary-scale atmospheric phenomena associated with the Southern Oscillation. *Mon. Wea. Rev.*, **109**, 813–829.
- Hoskins, B. J., and D. J. Karoly, 1981: The steady linear response of a spherical atmosphere to thermal and orographic forcing. *J. Atmos. Sci.*, **38**, 1179–1196.
- Houghton, J. T., G. J. Jenkins, and J. J. Ephraums, Eds., 1990: *Climate Change, The IPCC Scientific Assessment*. Cambridge University Press, 365 pp.
- Humphreys, W. J., 1940: *Physics of the Air*. Dover, 676 pp.
- Jones, P. D., 1988: The influence of ENSO on global temperatures. *Climate Monitor*, **17**, 80–89.
- , and P. M. Kelly, 1988: Causes of interannual global temperature variations over the period since 1861. *Long and Short Term Variability of Climate. Lecture Notes in Earth Sciences 16*, H. Wanner and U. Siegenthaler, Eds., Springer-Verlag, 18–34.
- , and K. R. Briffa, 1992: Global surface air temperature variations during the twentieth century: Part 1, spatial, temporal and seasonal details. *The Holocene*, **2**, 165–179.
- , S. C. B. Raper, R. S. Bradley, H. F. Diaz, P. M. Kelly, and T. M. L. Wigley, 1986a: Northern Hemisphere surface air temperature variations: 1851–1984. *J. Climate Appl. Meteor.*, **25**, 161–179.
- , —, and T. M. L. Wigley, 1986b: Southern Hemisphere surface air temperature variations: 1851–1984. *J. Climate Appl. Meteor.*, **25**, 1213–1230.
- , —, and —, 1986c: Global temperature variations between 1861 and 1984. *Nature*, **322**, 430–434.
- , T. M. L. Wigley, and G. Farmer, 1991: Marine and land temperature data sets: A comparison and a look at recent trends. *Greenhouse-Gas-Induced Climatic Change: A Critical Appraisal of Simulations and Observations*, M. E. Schlesinger, Ed., Elsevier, 153–172.
- Khmelevtsov, S. S., D. I. Busygina, and Yu. G. Kaufman, 1995: Modelling of the spatial and temporal distribution of the stratospheric aerosol optical characteristics of volcanic origin. *J. Geophys. Res.*, submitted.
- Kirchner, I., and H. F. Graf, 1995: Volcanos and El Niño—signal separation in winter. *Climate Dyn.*, submitted.
- Kodera, K., 1993: Influence of the stratospheric circulation change on the troposphere in the Northern Hemisphere winter. *The Role of the Stratosphere in Global Change*, M. L. Chanin, Ed., NATO ASI Ser., Vol 18, Springer-Verlag, 227–243.
- Kondo, J., 1988: Volcanic eruptions, cool summers, and famines in the Northeastern part of Japan. *J. Climate*, **1**, 775–788.
- Lacis, A. A., J. E. Hansen, and M. Sato, 1992: Climate forcing by stratospheric aerosols. *Geophys. Res. Lett.*, **19**, 1607–1610.
- Lamb, H. H., 1970: Volcanic dust in the atmosphere; with a chronology and assessment of its meteorological significance. *Phil. Trans. Roy. Soc. London*, **A266**, 424–533.
- , 1977: Supplementary volcanic dust veil index assessments. *Climate Monitor*, **6**, 57–67.

- , 1983: Update of the chronology of assessments of the volcanic dust veil index. *Climate Monitor*, **12**, 79–90.
- Livezey, R. E., and W. Y. Chen, 1983: Statistical field significance and its determination by Monte Carlo techniques. *Mon. Wea. Rev.*, **111**, 46–59.
- , and K. C. Mo, 1987: Tropical–extratropical teleconnections during the Northern Hemisphere winter. Part II: Relationships between monthly mean Northern Hemisphere circulation patterns and proxies for tropical convection. *Mon. Wea. Rev.*, **115**, 3115–3132.
- Mass, C. F., and D. A. Portman, 1989: Major volcanic eruptions and climate: A critical evaluation. *J. Climate*, **2**, 566–593.
- McCormick, M. P., and R. E. Veiga, 1992: SAGE II measurements of early Pinatubo aerosols. *Geophys. Res. Lett.*, **19**, 155–158.
- Mitchell, J. M., Jr., 1961: Recent secular changes of the global temperature. *Ann. N. Y. Acad. Sci.*, **95**, 235–250.
- , 1970: A preliminary evaluation of atmospheric pollution as a cause of the global temperature fluctuation of the past century. *Global Effects of Environmental Pollution*, S. F. Singer, Ed., Reidel, 139–155.
- Newhall, C. G., and S. Self, 1982: The volcanic explosivity index (VEI)—an estimate of explosive magnitude for historical volcanism. *J. Geophys. Res.*, **87**, 1231–1238.
- Ramanathan, V., 1988: The greenhouse theory of climate change: A test by inadvertent global experiment. *Science*, **240**, 293–299.
- Rampino, M. R., and S. Self, 1984: Sulphur-rich volcanic eruptions and stratospheric aerosols. *Nature*, **310**, 677–679.
- Rasmusson, E. M., and T. H. Carpenter, 1982: Variations in tropical sea surface temperature and surface wind fields associated with the Southern Oscillation/El Niño. *Mon. Wea. Rev.*, **110**, 354–384.
- Rind, D., N. K. Balachandran, and R. Suozzo, 1992: Climate change and the middle atmosphere. Part II: The impact of volcanic aerosols. *J. Climate*, **5**, 189–208.
- Robock, A., 1978: Internally and externally caused climate change. *J. Atmos. Sci.*, **35**, 1111–1122.
- , 1979: The “Little Ice Age”: Northern Hemisphere average observations and model calculations. *Science*, **206**, 1402–1404.
- , 1981a: A latitudinally dependent volcanic dust veil index, and its effect on climate simulations. *J. Volcanol. Geotherm. Res.*, **11**, 67–80.
- , 1981b: The Mount St. Helens volcanic eruption of 18 May 1980: Minimal climatic effect. *Science*, **212**, 1383–1384.
- , 1983: Ice and snow feedbacks and the latitudinal and seasonal distribution of climate sensitivity. *J. Atmos. Sci.*, **40**, 986–997.
- , 1984a: Climate model simulations of the effects of the El Chichón eruption. *Geophys. Int.*, **23**, 403–414.
- , 1984b: Snow and ice feedbacks prolong effects of nuclear winter. *Nature*, **310**, 667–670.
- , 1991: The volcanic contribution to climate change of the past 100 years. *Greenhouse-Gas-Induced Climatic Change: A Critical Appraisal of Simulations and Observations*, M. E. Schlesinger, Ed., Elsevier, 429–444.
- , and M. Matson, 1983: Circumglobal transport of the El Chichón volcanic dust cloud. *Science*, **221**, 195–197.
- , and J. Mao, 1992: Winter warming from large volcanic eruptions. *Geophys. Res. Lett.*, **19**, 2405–2408.
- , and Y. Liu, 1994: The volcanic signal in Goddard Institute for Space Studies three-dimensional model simulations. *J. Climate*, **7**, 44–55.
- , and M. P. Free, 1995: Ice cores as an index of global volcanism from 1850 to the present. *J. Geophys. Res.*, **100**, in press.
- Ropelewski, C. F., and P. D. Jones, 1987: An extension of the Tahiti–Darwin Southern Oscillation index. *Mon. Wea. Rev.*, **115**, 2161–2165.
- Sato, M., J. E. Hansen, M. P. McCormick, and J. B. Pollack, 1993: Stratospheric aerosol optical depths, 1850–1990. *J. Geophys. Res.*, **98**, 22 987–22 994.
- Schönwiese, C.-D., 1988: Volcanic activity parameters and volcanism–climate relationships within recent centuries. *Atmosfera*, **1**, 141–156.
- Simkin, T., L. Siebert, L. McClelland, D. Bridge, C. Newhall, and J. H. Latter, 1981: *Volcanoes of the World*. Hutchinson Ross, 240 pp.
- Stowe, L. L., R. M. Carey, and P. P. Pellegrino, 1992: Monitoring the Mt. Pinatubo aerosol layer with NOAA/11 AVHRR data. *Geophys. Res. Lett.*, **19**, 159–162.
- Strong, A. E., 1984: Monitoring El Chichón aerosol distribution using NOAA-7 satellite AVHRR sea surface temperature observations. *Geophys. Int.*, **23**, 129–141.
- Wright, P. B., T. P. Mitchell, and J. M. Wallace, 1985: Relationships between surface observations over the global oceans and the Southern Oscillation. NOAA Data Rep. ERL PMEL-12, 61 pp.
- Xu, Q., 1988: The abnormally cold summers of central China and their relation to volcanic eruptions. *Aerosols and Climate*, P. Hobbs and M. Patrick McCormick, Eds., Deepak, 223–232.
- Yamamoto, R., T. Iwashima, and M. Hoshiiai, 1975: Effects of the surface air temperature averaged over the Northern Hemisphere and large volcanic eruptions during the year 1951–1972. *J. Meteor. Soc. Japan*, **53**, 482–486.
- Zwiers, F. W., 1987: Statistical consideration for climate experiments. Part II: Multivariate tests. *J. Climate Appl. Meteor.*, **26**, 477–487.